International Journal of Applied Earth Observations and Geoinformation 109 (2022) 102791

Contents lists available at ScienceDirect

International Journal of Applied Earth Observations and Geoinformation

journal homepage: www.elsevier.com/locate/jag

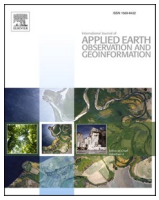

Proposal for an index of roads and structures for the mapping of non-vegetated urban surfaces using OSM and Sentinel-2 data

Eduardo Felix Justiniano [a,*], Edimilson Rodrigues dos Santos Junior [b], Breno Malheiros de Melo [b], João Victor Nascimento Siqueira [c], Rúbia Gomes Morato [a], Marcel Fantin [d], Julio Cesar Pedrassoli [e], Marcos Roberto Martines [f], Fernando Shinji Kawakubo [a]

[a] University of São Paulo – USP, Department of Geography, Brazil
[b] University of São Paulo – USP, São Carlos School of Engineering, Brazil
[c] Vale Institute of Technology Sustainable Development – ITV, Brazil
[d] University of São Paulo – USP, School of Architecture and Urbanism, Brazil
[e] Federal University of Bahia – UFBA, School of Engineering, Brazil
[f] Federal University of São Carlos – UFScar, Department of Geography, Tourism and Humanities, Brazil

ARTICLE INFO

Keywords:
OpenStreetMap
Volunteered geographic information
Google Earth Engine
Urban environment
Image classification

ABSTRACT

The use of volunteered geographic information (VGI), such as OpenStreetMap (OSM), to assist in mapping land use and coverage together with remote sensing images is relatively recent. Most studies have used OSM to assist in sample collection for image classification or aggregated vectors of buildings, transport, and land-use and coverage as ancillary data to support mapping refinements. This study proposes a metric called the "index of roads and structures" (IRS) created on the basis of OSM data with the intention of assisting in the mapping of non-vegetated and non-aquatic urban surfaces. IRS thresholds were defined and supplemented with information derived from the Normalized Difference Vegetation Index (NDVI) and the Modified Normalized Difference Water Index (MNDWI) as a way of extending the restriction between urban and non-urban classes and thus achieving better mapping accuracy. To implement this study, multispectral Sentinel-2 images resampled to 10 m on the ground were processed in the Google Earth Engine (GEE). The IRS is a raster file, in which each pixel is associated with the possibility of being inserted in an urban context; thus, the importance of this index as an aid in mapping urban areas is clear. We have demonstrated the possibility of using the IRS to map non-vegetated urban surfaces in Brazil (8.5 million square kilometers) and obtained a very high accuracy of 91.2%.

1. Introduction

There is no consensus on the definition of urban surfaces. There are countries where population density is the criterion for defining these areas. In other places, the characterization of an urban area considers urban settlements where a significant proportion of the population engages in non-agricultural activities (Zhu, 2019). As a rule, urban settlements are large groups of constructions where secondary and tertiary production are predominant (Stone, 1965). For Pesaresi et al. (2016), human settlements consist of population and physical structures. The constructions and buildings are essential parts of the physical infrastructure of the urban settlements, as are vegetated areas used as parks and lawns (Zhao and Zhu, 2022). All of these physical structures, in fact, are observed by remote sensing as material arrangements with electromagnetic properties that permit the measurement and characterization of the environment.

The mapping of urban areas using remote sensing is not a trivial task. The difficulty is partly due to the rich diversity of deposited materials—constructed or not—with different colors and arrangements, which makes this environment particularly complex. Pixels of any size in urban environments may contain a mixture of surface coverings with different spectral signals (Wentz et al., 2014). Hidden behind this "physical" complexity is another complexity: one that influenced the expansion of the city, linked to natural, historical and economic factors (Venturi, 2021).

In practical terms, to extract information using remote sensing images, the diversity of materials present in the urban environment is interpreted through its spectral properties (Harolds and Roberts, 2010).

* Corresponding author.
E-mail address: e.justiniano@alumni.usp.br (E. Felix Justiniano).

https://doi.org/10.1016/j.jag.2022.102791
Received 31 January 2022; Received in revised form 13 April 2022; Accepted 15 April 2022
Available online 30 April 2022

Different segments of the city may have more or less spectral diversity depending on the parceling of the land and the type of use linked to physical and social conditions. The complexity of mapping urban areas is also linked to the characteristics of the images used in mapping, since, depending on the instrument configuration, specific details in terms of spectral signatures and spatial dimensions are recorded.

One very rational and efficient methodology of analysis has been presented by Ridd (1995), who proposed that the urban environment consists of vegetation, impermeable areas and exposed soil (the V-I-S model), but aquatic surfaces are disregarded. The great advantage of the V-I-S model is that it makes it possible to analyze the structure of the territory (neighborhoods, districts, etc.) via the presence of these three components in the landscape, also making it possible to link these components to the prevailing social, economic and functional conditions in the space. Another advantage is that the V-I-S model uses various sources of input data (aerial photographs and orbital images with different levels of resolution) and forms of extracting thematic information.

Approaches both to the classification of images and the enhancement of components, as well as hybrid strategies (enhancement followed by classification) are widespread in the mapping of urban areas. The advantages and disadvantages of each are well described in the literature (Lu and Weng, 2007; Mesev, 2010; Jensen, 2016).

The advent of the possibility of sharing volunteered geographic information, in which the user generates content on the Internet, has created new horizons in urban studies (Goodchild, 2007). OpenStreetMap (OSM) has been formed in a community effort to map the world using a platform in which natural elements and human infrastructure are defined and labeled (Albrecht, 2020). Recently, various studies have used OSM in conjunction with remote sensing images and other data sources with the aim of mapping urban areas. It can be seen from Table 1 that most of these studies used OSM data to assist in the collection of samples in the classification of images or made use of the features available as an additional data source (ancillary data) to be incorporated into their studies.

In these studies, OSM data helped in the selection of plots, points of interest and semantic objects, which were used as a reference for image processing. The present research proposal, however, differs from the above-mentioned works, since it seeks to integrate the OSM data with the remote-sensing images to produce an index that can be applied to mappings.

Faced with the challenge of mapping urban areas and the importance of this information in territorial planning, this study proposes a new metric called the index of roads and structures (IRS) created from OSM data and spectral indices. To demonstrate the efficiency of the index, we selected the entire territorial expanse of Brazil with its 8,514,876 km^2 as a test area. Brazil was selected as a study area because it includes a very complete showcase of the main landscapes and ecologies of the tropical world (Ab'Sáber, 2002), into which urban areas are inserted.

2. Materials and methods

2.1. Analysis platform and satellite data

The data from the OSM were obtained from the Geofabrik platform (https://download.geofabrik.de/south-america/brazil.html) on dates between 03/29/2021 and 04/04/2021, so that there would be no major variations between the versions of the files provided by Geofabrik. ArcGIS software version 10.2 was used to select polygons and features, to pre-process them and for the conversion to raster files.

The cloud-image processing platform Google Earth Engine (GEE, Google Inc.) was used to process rasterized OSM files and orbital images (Fig. 1). To map the details of urban surface areas, we chose to use Sentinel-2 images from 2020, standardizing the data set to 10-meter

Table 1
Studies aimed at mapping urban areas using OSM data.

Authors	Area	Remote sensing imagery and statistics, mapping and other data	Detection of water and vegetation	OSM procedures
Arsanjani et al. (2013)	Central part of the City of Vienna (32 km^2)	Global Monitoring for Environment and Security Urban Atlas	OSM and GMESUA layers	Land segmentation to assist in mapping without use of remote sensing
Yang et al. (2017)	Southeastern United States (North Florida and South Georgia, approximately 185 km^2)	Landsat 8, Forest Canopy Height, MODIS 13 EVI, Shuttle Radar Topography Mission (SRTM), geospatial land ownership data, Google Earth	NDVI, OSM (waterways, bodies of water)	Use of the polygon centroids as samples in the Random Forest classifier
Chen et al. (2018)	Beijing (16,808 km^2)	GaoFen-2, selected points of interest from Amap (https://www.amap.com)	Support Vector Machine (SVM) for vegetation	Elimination of road redundancy and buffer for parcel definition
Zhao et al. (2019)	Beijing (56 km^2)	WorldView-2	NDVI	Integration with WorldView 3 for extracting semantic information
Qiao et al. (2019)	Beijing (16,808 km^2)	GaoFen-1, Air Quality Index of Beijing Municipal Environmental Monitoring Center, Third National Economic Census of Beijing, Amap	SVM to identify vegetation	Use of roads to delimit parcels with subsequent elimination of the roads
Liu et al. (2020)	Middle Yangtze River basin (317,000 km^2)	Landsat, OSM, Hansen Global Forest Change, Geo-Wiki, field photos, DEM (SRTM), Google Earth, Global Geo-referenced Field Photo Library	NDVI, MNDWI, Normalized Difference Built-up Index (NDBI), Built-up Index (BuEI), Soil Index (SoEI)	Selection of polygons of interest for obtaining land-use samples and kernel density of major roads
Zhang, Gorelick and Zimba (2020)	Corpus Christi-Kingsville metropolitan region in South Texas (around 170 km^2)	Landsat 5, Landsat 7, Landsat 8, National Wetland Inventory (NWI) maps and National Agricultural Statistics Service	NDVI and Normalized Difference Water Index (NDWI)	Vertices of the polylines of roads and constructions centroid as samples of impermeable surfaces
Sun et al. (2020)	Nanjing (1,624 km^2)	Sentinel-2, Landsat, Luojia-01, Google Earth high-resolution image, Amap, FROM-GLC10, Bigemap, mobile phone locating-request	NDVI	Road buffer definition of parcels, together with information on aquatic surfaces and impermeable surfaces
Zhong et al. (2020)	Six areas of Beijing, Wuhan, Macao and Hong Kong, the largest being 886 km^2.	Amap, Google Earth	OSM water layers	Use of roads as semantic objects and for the determination of land parcels
Chen et al. (2021)	Metropolitan areas of San Francisco, Denver, New Orleans, Chicago and New York City.	Sentinel-1, Sentinel-2, VIIRS, National Agriculture Imagery Program (NAIP) and National Elevation Data, Global Urban Boundary (GUB), Google Earth Imagery, Google Street View, WorldPop and Twitter	NDVI and NDWI	Use of the principal and secondary roads to define land parcels

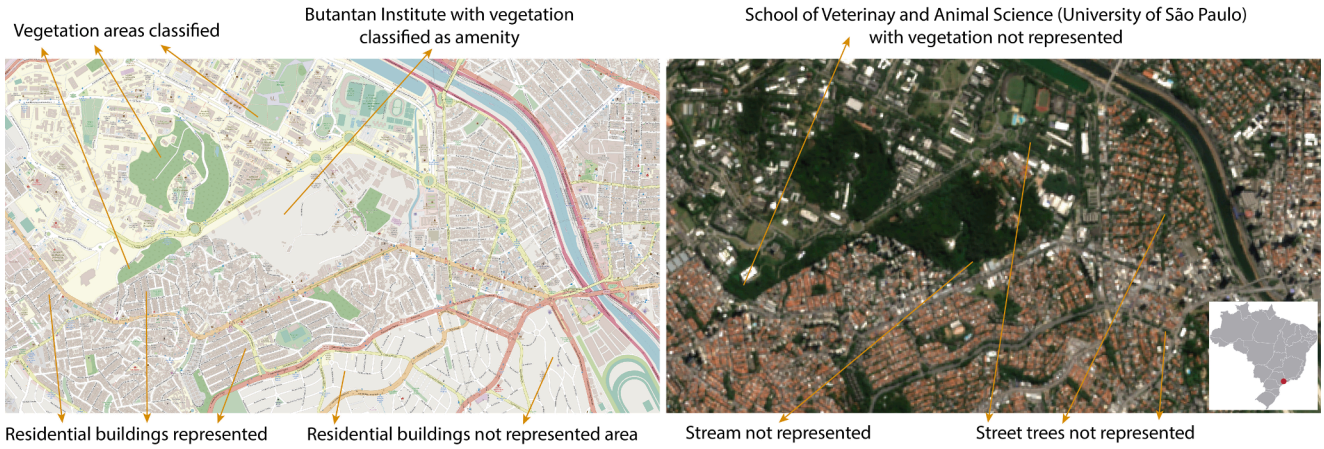

Fig. 1. Data available in OSM (2021) and the Sentinel-2 color rendering (4R3G2B) of 2020 in the Butantã District and part of the Campus of the University of São Paulo, in the city of São Paulo, SP. As can be seen, the OSM polygons did not include all the green areas. On the other hand, OSM has delimitations of areas, such as land use, that cannot be easily delimited in images. (For interpretation of the references to color in this figure legend, the reader is referred to the web version of this article.)

spatial resolution. As pre-processing steps, the images were filtered to eliminate clouds and considering a maximum cloud cover of 40% of the scene. Values below 40% were considered too restrictive for some localities, such as in the Caatinga biome (in the Northeast region), which would prevent the analysis of the images collected in wet seasons—a very important aspect for implementing the proposal. In total, the analysis considered 42,578 Sentinel-2 scenes in an area corresponding to 85 billion pixels.

2.2. Construction of the index of roads and structures (IRS)

The IRS is a composite index that aggregates information from the OSM, more specifically from road, building, land-use and transport features. Two stages were adopted for the construction of the IRS. The first step consisted of calculating the density of roads; in the second stage, information related to the type of land use and transport was selected. These were incorporated into the IRS in two ways: the density of contour polylines and a constant value (offset), assigned to the selected land-use and transport polygons. This constant value was necessary because some areas have dimensions that exceed the influence radius of the kernel function. This constant value must be large enough to ensure that structures are represented in the mapping. To be compatible with the resolution of Sentinel-2 images, the pixel size considered for generating the density raster file was 10 meters.

For the calculation of the road density, as well as for the calculation of the density of perimeters of the land-use and transport features, the following formula, adapted from Silverman (1986, Eq. 4.5), was used (Eq. (1)):

$$\text{density} = \frac{\sum_{i=0}^{n} L_i P_i}{\pi r^2} \quad (1)$$

Where:
r = influence radius;
L_i = length of lines in the radius of influence;
P_i = Population field value.

The observation of the territory was important for determining the values of the radius of influence. In Brazil, as in other countries, the greatest distances between urban roads are found in industrial, commercial, storage or transportation areas, whose structures can be represented in OSM. Apart from these areas, the greatest distances between urban roads in Brazil are found in the pilot plan of Brasilia, capital of Brazil, where the maximum distance observed between roads of blocks not covered by water or vegetation was 160 m.

The first measured kernel line density influence-radius value was less than this distance at 0.0010° (≈100 m). From this value, increments of 0.0005° (≈50 m) in the radius of influence were added. The default value of the kernel density is that associated with an isolated and straight-line stretch of road. The adjustment of the radius of influence should aim to minimize occurrences of values below the default value between urban roads and above the default between non-urban roads.

Thus, in this study, considering the extent, complexity and latitudinal range of the Brazilian territory, the influence radius of 0.002 degrees (≈200 m) proved to be satisfactory for the intended adjectives, since the values among urban roads were mostly higher than the value obtained for a single road, whereas in rural roads, the values found were predominantly lower.

For the calculation of the density for buildings, the composite features were divided and a limit for the perimetral length was established. Of the land-use and transport vectors, only the features associated with the urban context were considered (Table 2).

Many areas represented by land-use and transport features, such as military areas and airports, have high proportions of aquatic or vegetation coverage. In such cases, it was necessary to restrict these features, eliminating areas covered by vegetation and water. The remaining individual features, whose perimeters also exceeded 200 m, were added to the building features, which were transformed into polylines. Subsequently, the same kernel density calculation as applied to roads was used (Eq. (1)).

In most of Brazil, it may be sufficient to consider only the density of roads when producing the IRS. However, OSM contains representations of areas of large structures or areas where there is a set of structures with few access routes (Fig. 2A, B and C). In this case, and in order to improve the effectiveness of the proposed index, it becomes valid to enter information from these areas by means of the kernel line density of the perimeter of these areas (Fig. 2D) and a constant value of the area, transformed into a raster image (Fig. 2E). The result can be obtained by summing the values of each pixel or by choosing the maximum value between the pixels of the images (Fig. 2G).

Table 2
OSM polygon classes used for the construction of the IRS.

Vectors	Classes used
Building	All individual features with a perimeter of 200 m or more.
Land use	Cemetery, commercial, industrial, military, recreation ground, retail
Transport	Airfield, airport, apron, bus_station, ferry_terminal, helipad, railway_station

Source: Geofabrik (2021).

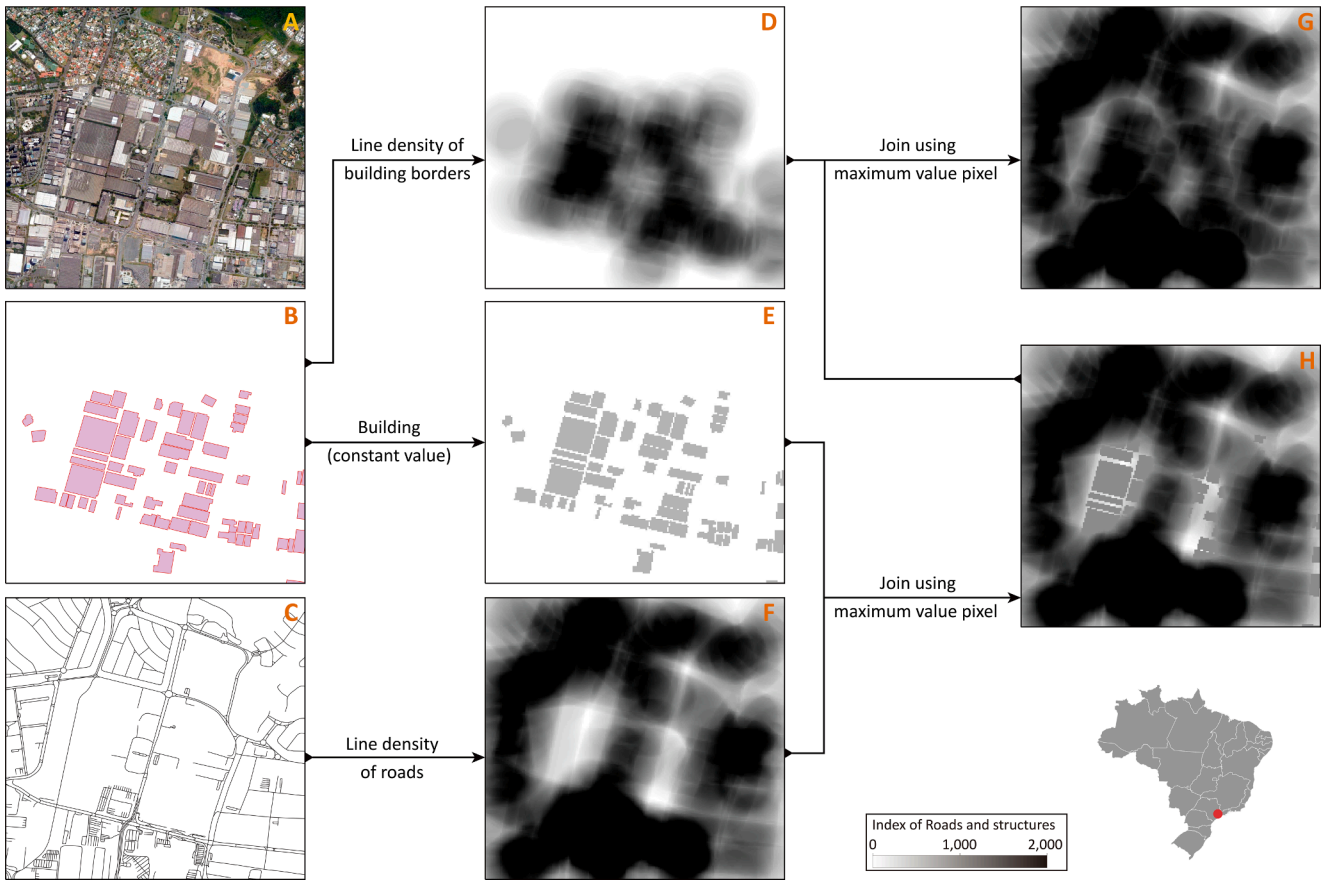

Fig. 2. Roads and structures from OSM and IRS composition in the industrial area of Alphaville, Municipality of Barueri, SP (2021). The importance of using the polygon information for constructions (G and H) in the composition of the IVE is observed. The offset value used was 800, without which the construction cannot be represented in mapping with the IRS.

2.3. Exclusion of vegetated and aquatic surfaces

High values of IRS are closely associated with the presence of urban settlements, but the index does not exclude vegetated and aquatic surfaces. Thus, as a complement to the IRS, the Normalized Difference Vegetation Index (NDVI; ROUSE et al. 1973) and Modified Normalized Difference Water Index (NDWI; XU, 2006) spectral indices were used to impose restrictions. While NDVI (Eq. (2)) provides an indication of biomass above the ground, MNDWI (Eq. (3)) emphasizes features of bodies of water in addition to decreasing the correlation of water with features associated with built areas. The formulas adopted for Sentinel-2 were:

$$\mathrm{NDVI} = \frac{\mathrm{B8} - \mathrm{B4}}{\mathrm{B8} + \mathrm{B4}} \tag{2}$$

$$\mathrm{MNDWI} = \frac{\mathrm{B3} - \mathrm{B11}}{\mathrm{B3} + \mathrm{B11}} \tag{3}$$

Where:

B3 = pixel values of the green band, centered on 560 nm;

B4 = pixel values of the red band, centered on 665 nm;

B8 = pixel values of the near infrared band, centered on 842 nm and.

B11 = pixel values of the short-wave infrared band, centered on 1,610 nm.

In order to highlight the differences in signatures, maximum values of NDVI and MNDWI constructed from a temporal set of 42,578 Sentinel-2 images obtained for all of Brazil at different times in 2020 were considered in the analysis. The cut-off values defined in the composition of the IRS for the NDVI and MNDWI indices were 0.5 and 0.2, respectively. By adopting this strategy of using temporal composites ($\mathrm{NDVI_{max}}$ and $\mathrm{MNDWI_{max}}$), much class-to-class confusion was reduced due to the coverage's own development characteristics, which permits a better separation between classes.

2.4. Methodological proposal for mapping non-vegetated urban surfaces

Fig. 2 shows a model for composing the IRS (Fig. 3A) and its use, supplemented with information from the NDVI and MNDWI (Fig. 3B and C). This model has been used to map urban surface areas of Brazil and can be replicated for different areas of the globe, provided that information from the OSM is available and has details that allow the features to be associated with the urban infrastructure.

For the composition of the IRS (Fig. 3A), a higher value among urban roads and a lower value among rural roads should occur, taking as reference the value of an isolated road for the same influence radius.

The establishment of NDVI and MNDWI thresholds (Fig. 3B) was first used to establish restrictions on transport and land-use features, eliminating water- and vegetation-covered surfaces. In a second step (Fig. 3C), the thresholds of these indices were used to restrict the IRS image. The NDVI and MNDWI thresholds, which can be defined in the steps described in Fig. 3B and C, are not necessarily the same, neither is the maximum cloud cover threshold. Maximum cloud cover and thresholds of NDVI, MNDWI and IRS, with values of 10; 0.5; 0.2 and 600, respectively, were established to produce the first mapping of Brazil with the IRS. In this, the boundaries of non-vegetated and non-aquatic urban surface areas were defined.

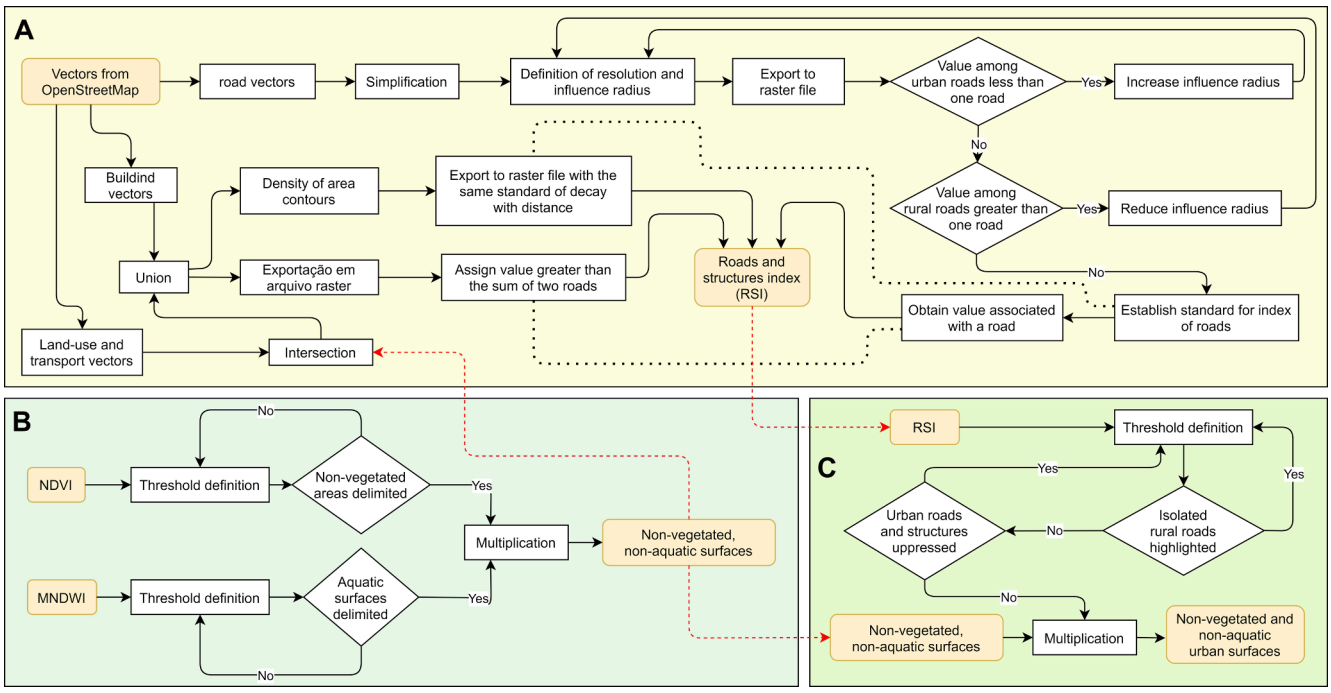

Fig. 3. Model for mapping non-vegetated and non-aquatic urban surfaces.

2.5. Mapping accuracy

In order to evaluate the accuracy of mapping of non-vegetated urban surfaces, 600 control points distributed in a stratified random manner were used, distributed in 300-meter-wide bands, established by means of buffers of urban settlement area limits, defined in the first mapping, that take Brazilian state capitals and surrounding areas into consideration. The total area of these bands was 2,437 km^2. These border areas were selected because they are areas with the greatest likelihood of omission and commission errors. For the classification of validation points, high-resolution images from Google Earth (Google Inc.), Google Street View, Sentinel-2 data and from the Planet satellites (Planet Labs PBC) were used (Fig. 4). Thus, samples were collected in various climates and biomes, distributed in broad latitudinal and longitudinal bands, including diversities of urban settlements within matrices of preserved areas, agricultural crops or pastures.

The use of IRS for mapping urban surfaces not covered by water or vegetation was evaluated at different thresholds of NDVI and MNDWI (Fig. 3B), IRS (Fig. 3C), maximum cloud cover and influence radius. We performed several classifications to evaluate the sensitivity (true positive rates of points classified as urban surface not covered by water or vegetation), specificity (true negative rates of points classified as water or vegetation) and accuracy (percentage of points correctly classified in relation to the total) of the mapping.

3. Results

3.1. Classification performance of the IRS

Visual analyses indicated the great potential of the IRS to improve

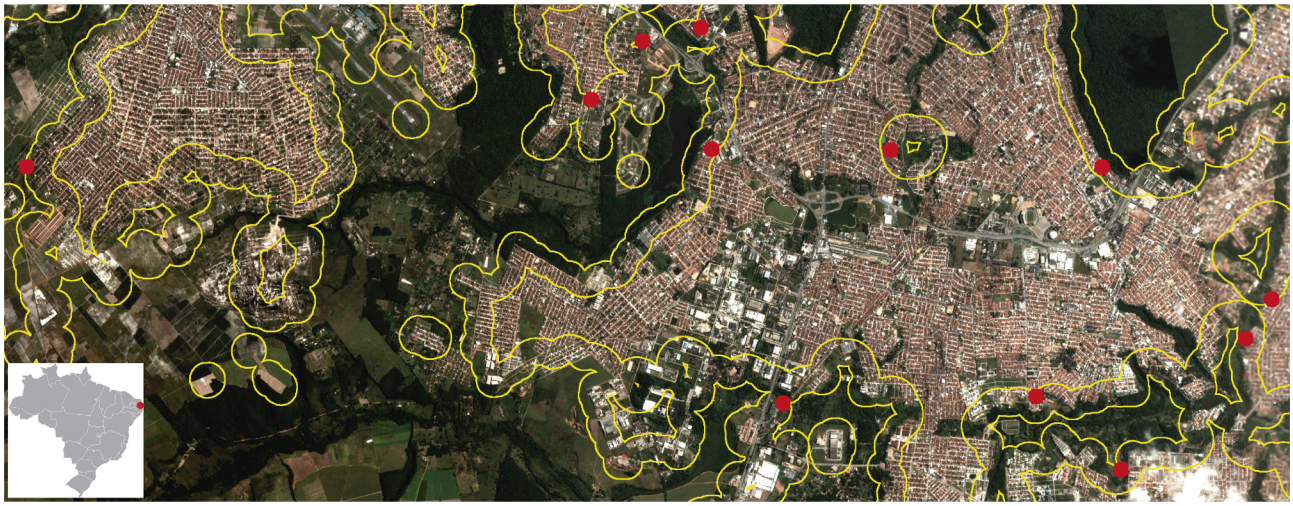

Fig. 4. Buffer of boundaries of urban surfaces (yellow) and stratified random validation points (red) overlaid on a real-color rendering from Planet in the Metropolitan Region of João Pessoa, State of Paraíba. (For interpretation of the references to color in this figure legend, the reader is referred to the web version of this article.)

the mapping of urban surfaces at different levels of agglomeration. The effectiveness of the index increased when complementary information obtained by spectral indices was incorporated into the analysis as a way of expanding the restrictions. Table 1 shows the results of the classifications adopting different thresholds for cloud, NDVI, MNDWI and IRS, and the respective performances obtained. As can be seen, the best result was found with Classification 15, since it gave the highest accuracy value (0.9117) and the lowest mean absolute deviation (0.0003). However, when NDVI and MNDWI information were not included in the classification (Classification 19), the accuracy of the mapping was much lower (0.5650) and with an absolute mean deviation well above the other classifications (0.2774).

As to the values of the kernel-function influence radius, it was found that the accuracy for radii from 0.0015 to 0.0025 was constant, but with little variation in the measures associated with omission and commission errors. This indicates that small variations in the influence radius cause little change in the result.

When comparing the IRS with the NDVI and MNDWI, a low linear correlation was observed (–0.2931 and –0.1255, respectively), indicating the non-redundancy of information among these indices to be considered in the mapping of urban areas (Fig. 5B, C and D). In other words, the low correlation is an indication that the information in the IRS is complementary to that obtained with the NDVI and MNDWI.

3.2. Non-vegetated urban surfaces mapping of municipalities

A mapping of urban surfaces of the municipalities of Porto Nacional and Palmas, capital of the State of Tocantins, not covered by water or vegetation, was produced (Fig. 5A) using the thresholds presented in Classification 15 (Table 3). This cut-off has relatively balanced proportions of water, vegetation and urban areas. The result was found to be quite satisfactory, showing different patterns in the distribution of the intra-urban vegetation and areas where the densities of roads and structures were higher.

It has been estimated that the total of urban surfaces not covered by water or vegetation occupied 43,265 km^2 of the Brazilian territory (Fig. 6). As can be seen, urban surfaces are not uniformly distributed across the country, with a lower concentration in the Pantanal and Amazon biomes. The highest concentrations occur in the Caatinga and Atlantic Forest biomes, with the main capitals and metropolitan regions of the country being located in the latter biome. The explanation for this regional pattern of occupation is due to the history of colonization of Brazil, which began from the coast and extended to the inland areas as colonization advanced. In the Cerrado and the Amazon, the most effective process of occupation was much more recent, being closely related to the large Amazon occupation projects implemented especially in the 1960s and 1970s (Becker, 1982). Currently, the regions of Cerrado in the Central-West have experienced urban growth driven by the expansion of agribusiness, with grain production and extensive cattle ranching.

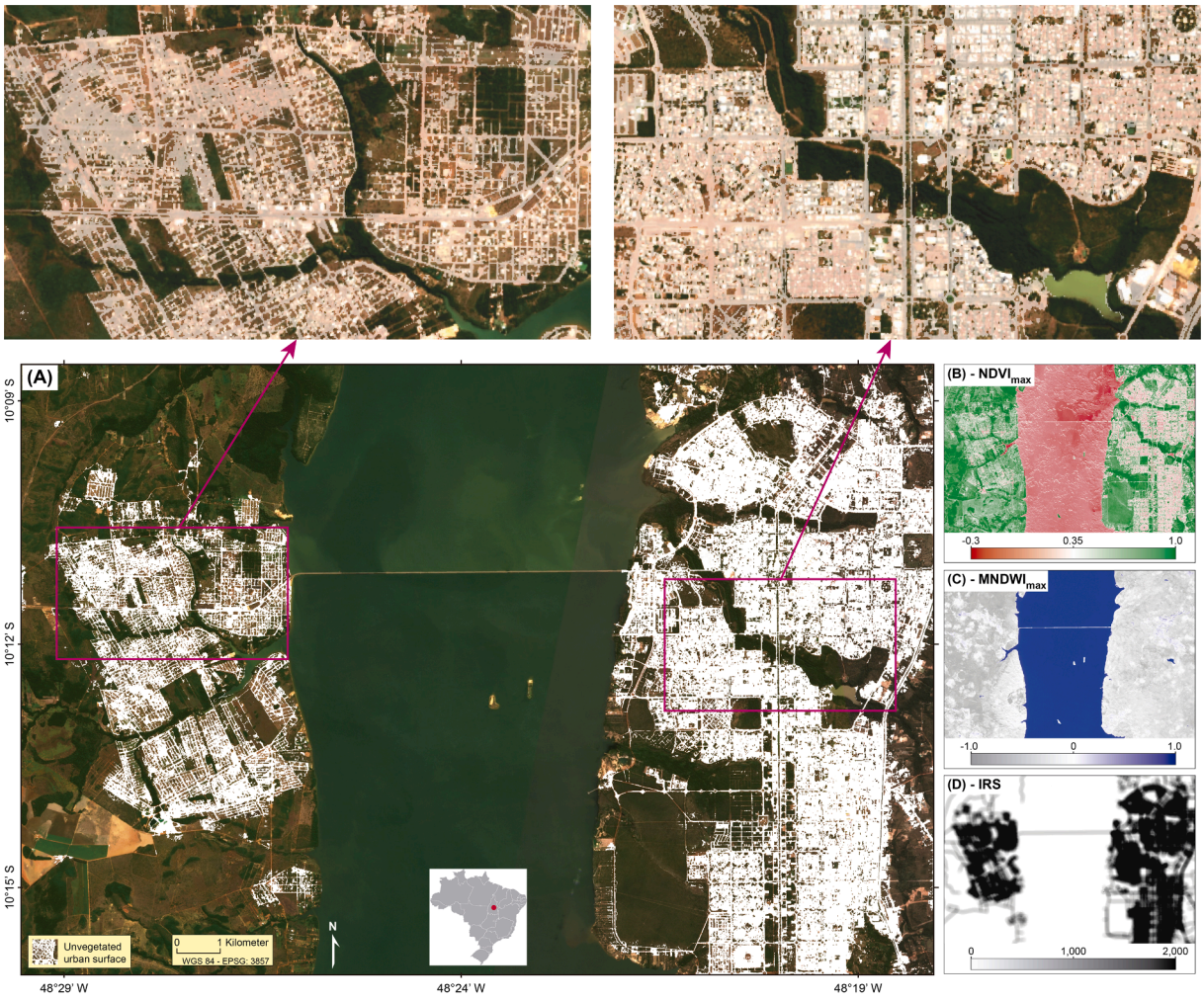

Fig. 5. Result of the mapping flow of non-vegetated urban surfaces (blank) overlaid on a real-color rendering from Planet.

Table 3
Thresholds used in the classifications and the performances obtained.

Classification	Cloud	NDVI	MNDWI	IRS	Radius (degrees)	Sensitivity	Specificity	Accuracy	Mean absolute deviation
1	10	0.5	0.2	600	0.0020	0.9392	0.8388	0.8883	0.0336
2	20	0.5	0.2	600	0.0020	0.9595	0.8026	0.8800	0.0525
3	30	0.5	0.2	600	0.0020	0.9595	0.7533	0.8550	0.0690
4	20	0.4	0.2	600	0.0020	0.9831	0.6382	0.8083	0.1155
5	40	0.5	0.2	600	0.0020	0.9595	0.7303	0.8433	0.0767
6	20	0.6	0.2	600	0.0020	0.9155	0.8816	0.8983	0.0114
7	20	0.7	0.2	600	0.0020	0.8378	0.9211	0.8800	0.0279
8	20	0.6	0.2	500	0.0020	0.9122	0.8980	0.9050	0.0047
9	20	0.6	0.2	550	0.0020	0.9155	0.8882	0.9017	0.0092
10	20	0.6	0.2	650	0.0020	0.9155	0.8553	0.8850	0.0202
11	20	0.6	0.1	500	0.0020	0.9155	0.8717	0.8933	0.0147
12	20	0.6	0.3	500	0.0020	0.9122	0.9079	0.9100	0.0014
13	20	0.6	0.4	500	0.0010	0.9223	0.8882	0.9050	0.0114
14	20	0.6	0.4	500	0.0015	0.9155	0.9079	0.9117	0.0026
15	**20**	**0.6**	**0.4**	**500**	0.0020	**0.9122**	**0.9112**	**0.9117**	**0.0003**
16	20	0.6	0.4	500	0.0025	0.8986	0.9243	0.9117	0.0086
17	20	0.6	0.4	500	0.0030	0.8953	0.9178	0.9067	0.0075
18	20	0.6	0.4	500	0.0035	0.8986	0.9145	0.9067	0.0053
19	**20**	**1**	**1**	**500**	0.0020	**0.1453**	**0.9737**	**0.5650**	**0.2774**

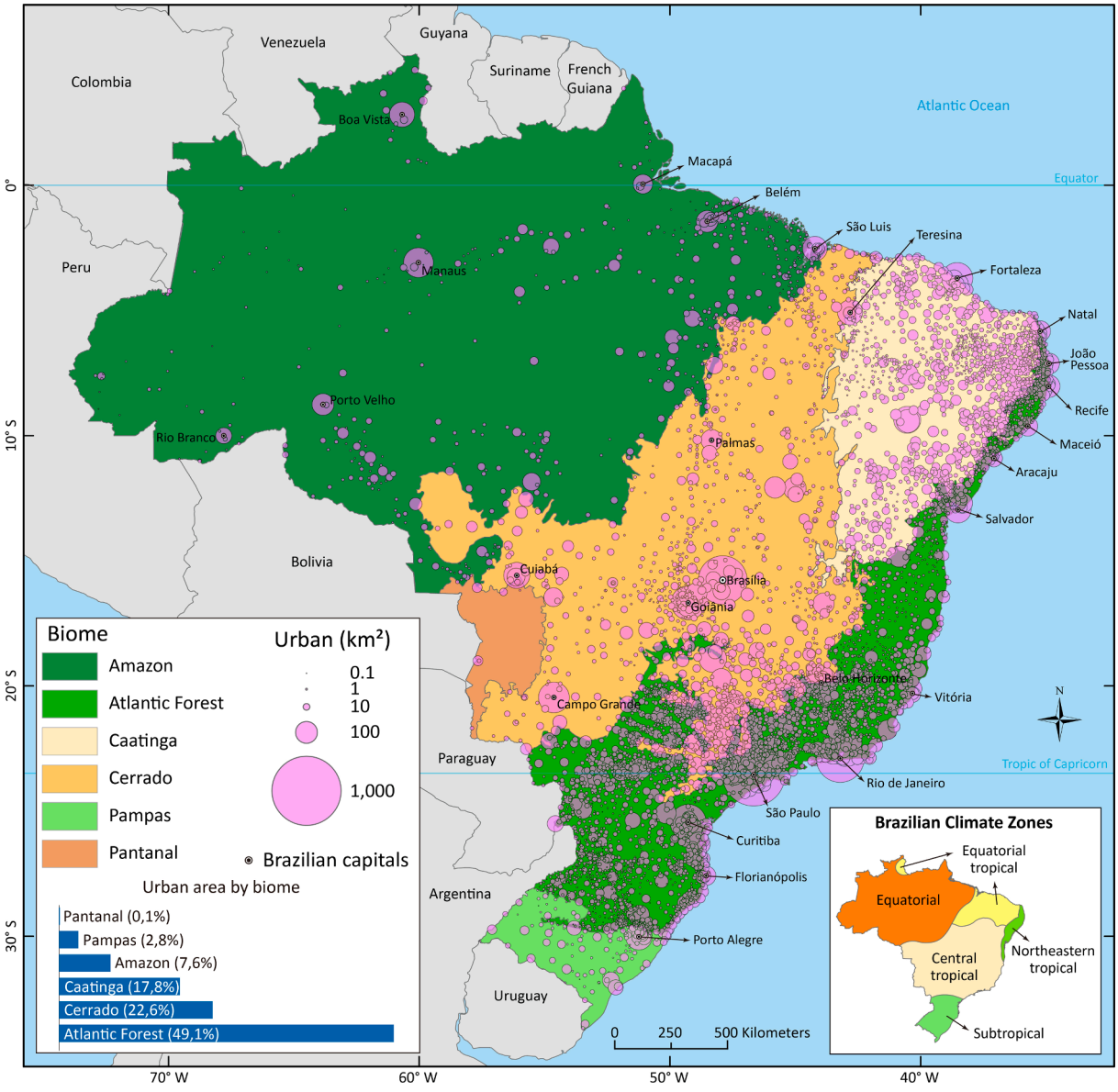

Fig. 6. Urban surface not covered by water or vegetation mapped to the 5568 municipalities of the Brazilian territory plus the Federal District (2020).

4. Discussion

4.1. OSM and IRS

Several studies have used OSM and remote sensing for urban mapping (see Table 1). As far as we can see, OSM was used to define samples (Yang et al., 2017; Liu et al., 2020; Zhang, Gorelick and Zimba, 2020), to determine land parceling (Chen et al., 2018; Chen et al., 2018; Sun et al., 2020; Zhong et al. 2020; Chen et al., 2021) and to assist in obtaining semantic objects (Zhao et al., 2019; Zhong et al., 2020), which were subsequently processed by artificial-intelligence algorithms for producing mappings, which delimit distinct classes. This research demonstrated the possibility of using data from OSM in conjunction with orbital images to map non-vegetated surfaces in extensive territorial areas, using relatively simple but robust techniques in terms of practical results.

The IRS can be considered to be a raster file, in which the value of each pixel is associated with the possibility of being part of the urban area. Its quality depends on the detail and completeness of surface objects representation in the vector files provided by Geofabrik. The high values of sensitivity, specificity and accuracy obtained in mapping (see Table 3) are indicative of the good quality of representation of roads, buildings and land use in OMS.

Another important point to mention is that there are areas and large buildings that are not represented in OSM. The absence of these elements imposes a certain limitation on the IRS, resulting in increments in omission errors. In this work, we used vectors published in March and April 2021 and Sentinel-2 images from 2020. Even with this temporal lapse, we observed buildings and areas not represented in OSM. A longer period of time between Sentinel-2 images and OSM data can mitigate but not eliminate the problem, since there are older constructions that were not represented in OSM (Fig. 2).

4.2. The V-I-S model

In Ridd's V-I-S model, the urban environment consists of vegetation, impermeable areas and exposed soil. The validation samples used in this study also identified these three elements, which predominate in the Brazilian landscape, together with a fourth that corresponds to aquatic surfaces. This composition reinforces the viability of the model proposed by Ridd (1995) to characterize, in a more detailed way, the intra-urban structure of Brazilian municipalities. Of the 600 validation points, 313 were located on an urban surface not covered by water or vegetation (buildings, roads, parking lots and others). Of these, 56 were exposed soil and four were sand. The increased occurrence of these surface materials in urban areas can be explained by the peripheral location of the sampling band, often in areas where cities are expanding.

4.3. Environmental conditions and the accuracy of the mapping

To achieve the accuracy of 91.2% mapping, IRS thresholds combined with maximum cloud cover, NDVI and MNDWI values were defined. We considered that this value followed a very rigid and conservative protocol, since reference samples used in the calculation of accuracy were collected over areas of higher tension, i.e., areas with greater chances of finding confusion between classes. It is therefore reasonable to assume that the "real" result for mapping accuracy tends to be greater than the value disclosed here. Another point observed is that commission and omission errors showed a difference of 0.0003 (see Classification 15, Table 3). In other words, when urban area calculations are aggregated by municipalities, the estimates obtained tend to converge to values closer to reality, since deviations associated with inclusion or exclusion errors tend to compensate one another when their values are approximately equal.

An important aspect to be considered in mapping large areas in a tropical environment concerns restrictions imposed by atmospheric conditions. For this, GEE played a crucial role, because it allowed not only the processing of a very large mass of data, but it also made it possible to produce synthetic images through the use of temporal reducers (Gorelick et al. 2017). Even using this resource, the atmospheric conditions observed in some parts of Brazil imposed limitations on the definition of the best thresholds to be adopted for classification. As can be seen in Table 3, the accuracy of Classification 1 was better than for Classification 2, suggesting that the maximum cloud cover limit of 10% would achieve better results. However, by adopting a lower threshold of atmospheric interference, 59 municipalities ended up with no urban area mapped within their territories. This problem was due to the lack of Sentinel-2 images with low cloud cover or cloud masking that returned pixels associated with urban areas without information, thus omitting these areas from the classification.

Of the Brazilian biomes, Caatinga (vegetation associated with a semi-arid climate located in the northeastern region of the country) required greater attention, considering the possible temporal series of 2020. In Caatinga, herbaceous plants only grow during the rainy season, as do grasses, which is why they are not apparent for most of the year (Rizzini, 1997p.515). For Ab'Sáber (2003), Caatinga often functions as a cloudy semi-desert, with everything reverting when the first rains arrive. As a result of this characteristic, restricting orbital images to scenes with little or no cloud would result in lower NDVI values, even considering annual maximum values. As an example, we can highlight the area of a company in the municipality of Sobral, in the state of Ceará (Fig. 7A). Using the maximum cloud cover limit of 10%, we found lower $NDVI_{max}$ values (Fig. 7B) than those found when using the 40% cloud cover limit (Fig. 7C). In this way, the cloud cover limit is also an important variable in the IRS configuration and in mapping with this index. Due to this particular characteristic, unlike the rest of Brazil, the threshold for selecting scenes of up to 40% cloud cover was adopted for the composition of the IRS for the states in the northeastern region.

Especially in the Caatinga and Cerrado biomes (northeastern and central-western regions), confusion in the classifications involving urban surfaces, senescent vegetation, exposed soils, sand banks and rocky outcrops is commonly reported in the reviews of local literature (Silva and Cruz, 2018), with these confusions being more pronounced in the dry period. Hence the decision to work with images preferably obtained in the wet period (Almeida Filho; Carvalho, 2010). The adoption of $NDVI_{max}$ and $MNDWI_{max}$ compositions acts in a similar way to images obtained in wet periods, with the advantage of selecting only pixels with higher temporal series values within a stack of images. This resource is very useful, for example, for reducing any effects on vegetation caused by atypical episodes of drought within the wet season.

The accuracy of the classification of non-vegetated urban surfaces was calculated for Brazil as a whole. However, it should be taken into consideration that there are areas where the model is well-adjusted and areas where commission errors are more evident, found along dual-track highways, junctions and rural areas with a higher density of roads and adjacent to rocky outcrops, of sandy surfaces and exposed soil.

An example of the occurrence of this error can be seen in the municipality of São José do Norte, in the State of Rio Grande do Sul (Fig. 8A). It is located in an estuarine plain with many junctions and high density of rural roads close to dunes. In addition, many streets in the urban area are sandy. Visually, commission errors were quite noticeable using the thresholds of Table 3 (Classification 15) (Fig. 8B). Changing the thresholds of NDVI and IRS to 0.45 and 600, respectively, reduced commission errors (Fig. 8C). Further expanding the restriction, we observed that on entering new information, such as night lights captured in the sensor images of the Visible Infrared Imaging Radiometer Suite (VIIRS), on board the Suomi NPP satellite, the commission errors decreased considerably (Fig. 8D). This indicates the need for more regional adjustments of the thresholds (as was done for the Caatinga biome) and reinforces the importance of using other sensors and information, aiming at an overall improvement of the mapping.

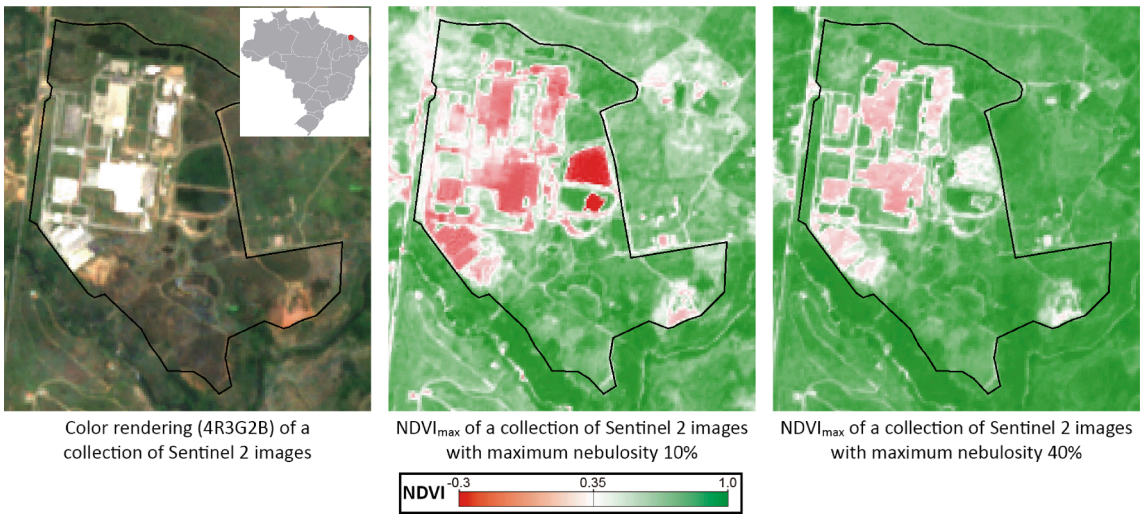

Fig. 7. Changing the $NDVI_{max}$ values relative to the maximum cloud cover of the Sentinel-2 scenes.

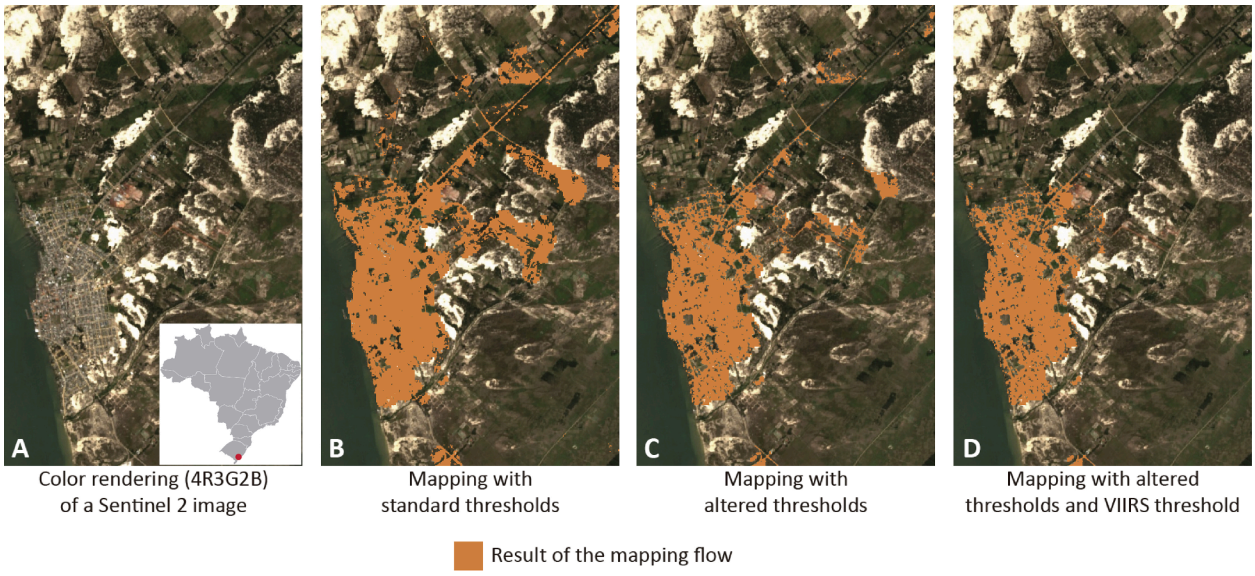

Fig. 8. Variations in the result of the mapping flow, related to the modification of thresholds, in the municipality of São José do Norte, RS (2020).

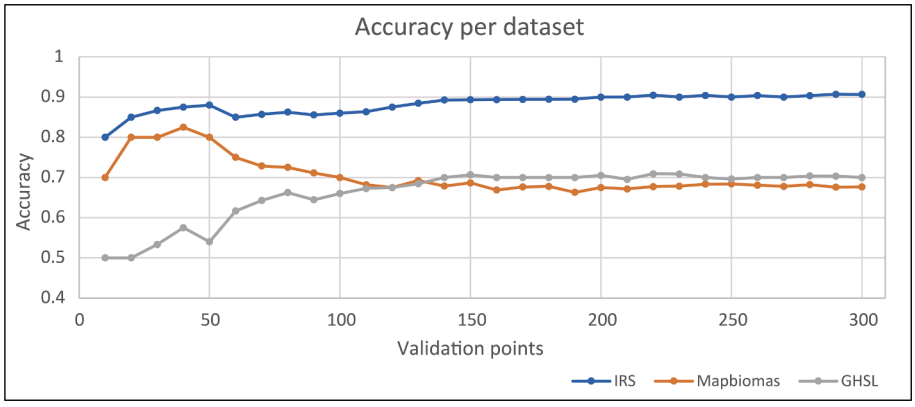

Fig. 9. Accuracy of IRS, Mapbiomes, and GHSL datasets. Validation was performed by selecting control samples randomly with replacement from the 600 samples available. All validations were performed independently.

4.4. Comparing IRS with MapBiomas and GHSL

Finally, comparing the results of the mapping produced with the IRS with the urban surfaces mapped by the MapBiomas Project (Souza Jr. et al., 2020) and Global Human Settlement Layer (GHSL) (Freire, 2019), we found that the accuracy obtained with our proposal was much greater. Fig. 9 illustrates the variation in accuracy obtained according to the increase in the number of control samples. A stabilization in accuracy values is observed in the three datasets with approximately 150 samples. However, whereas accuracy reaches approximately 0.7 in MapBiomas and GHSL, in IRS the level is much higher, reaching an accuracy of approximately 0.9. In addition, the accuracy values for the IRS were much more consistent throughout the series than the values observed for MapBiomas and GHSL.

Some hypotheses may explain such significant differences in the accuracy achieved in these datasets. Mapbiomas, for example, maps urban surfaces with a spatial resolution of 30 m (Souza Jr. et al., 2020) using Landsat images, while the IRS uses 10 m Sentinel-2 images. Moreover, in Mapbiomas, aquatic and vegetated surfaces within the urban patch are diluted as urban surfaces, resulting in an increase of divergence when the result is compared with control samples that consider only urban surfaces not covered by water and vegetation. In the case of GHSL, we used the pre-release version data package 2018 produced with Sentinel-1 data (Freire, 2019). The time lapse between the reference year of the samples (2020) and the GHSL may have caused a decrease in the accuracy of this dataset, especially because the validation points were obtained near the edges of the urban patches, in places where the expansion of cities is most evident. Despite the scenarios described, the IRS proved to be very efficient in mapping urban surfaces not covered by water or vegetation, bringing considerable gains in accuracy.

5. Conclusions

The use of the IRS, based on data from OSM, in conjunction with the NDVI and MNDWI, enabled the mapping of urban surfaces not covered by water or vegetation with high accuracy in Brazil for areas inserted into diverse biomes, distributed over a wide latitudinal and longitudinal range.

The IRS, $NDVI_{max}$, $MNDWI_{max}$ and maximum cloud cover thresholds of the Sentinel-2 scenes were shown to be important variables in the mapping process, without which the high accuracy would not have been achieved.

The high accuracy obtained when using the IRS is an indication that OSM data, combined with spectral indices, are appropriate for mapping urban areas.

The proposed methodology for mapping using the IRS made it possible to measure the areas of non-vegetated urban surfaces of all Brazilian municipalities, totaling 43,265 km^2.

CRediT authorship contribution statement

Eduardo Felix Justiniano: Conceptualization, Methodology, Software, Validation, Investigation, Data curation, Writing – original draft, Visualization. **Edimilson Rodrigues dos Santos Junior:** Validation, Writing – review & editing, Software. **Breno Malheiros de Melo:** Validation, Writing – review & editing, Software. **João Victor Nascimento Siqueira:** Data curation, Software. **Rúbia Gomes Morato:** Writing – review & editing. **Marcel Fantin:** Writing – review & editing. **Julio Cesar Pedrassoli:** Writing – review & editing, Validation, Software. **Marcos Roberto Martines:** Writing – review & editing, Formal analysis. **Fernando Shinji Kawakubo:** Supervision, Project administration, Writing – review & editing, Formal analysis.

Declaration of Competing Interest

The authors declare that they have no known competing financial interests or personal relationships that could have appeared to influence the work reported in this paper: [Eduardo Felix Justiniano reports financial support was provided by Coordenação de Aperfeiçoamento de Pessoal de Nível Superior (CAPES).].

Acknowledgements

The authors acknowledge the financial support of the Coordenação de Aperfeicoamento de Pessoal de Nível Superior [Coordination of Superior Level Staff Improvement] (CAPES) for the doctoral grant awarded to the first author of the article and thank the Mapbiomas project and the Cartography Laboratory of the Geography Department of the University of São Paulo.

Cordial thanks to the three anonymous reviewers for their valuable comments, which contributed greatly to the improvement of this manuscript.

GIS Operational procedures and Java Script files used in GEE are available at https://github.com/edujusti/IRS.

References

Ab'Saber, A.N., 2003. Os Domínios de Natureza no Brasil: potencialidades paisagísticas. Ateliê Editorial, São Paulo.

Albrecht, C.M., 2020. Change detection from remote sensing to guide OpenStreetMap labeling. ISPRS Int. J. Geo-Inf. 9 https://doi.org/10.3390/ijgi9070427.

Almeida-Filho, R., Carvalho, C.M., 2010. Mapping land degradation in the Gilbués region, northeastern Brazil, using Landsat TM images. Int. J. Remote Sens. 31, 1087–1094. https://doi.org/10.1080/01431160903260957.

Arsanjani, J.J., et al., 2013. Toward mapping land-use patterns from volunteered geographic information. Int. J. Geogr. Inf. Sci. 12, 2264–2278. https://doi.org/10.1080/13658816.2013.800871.

Becker, B.K., 1982. Geopolítica da Amazônia: a nova fronteira de recursos. Zahar, Rio de Janeiro.

Chen, B., et al., 2021. Mapping essential urban land use categories with open big data: Results for five metropolitan areas in the United States of America. ISPRS J. Photogramm. Remote Sens. 178, 203–218. https://doi.org/10.1016/j.isprsjprs.2021.06.010.

Chen, W., et al., 2018. Social functional mapping of urban green space using remote sensing and social sensing data. ISPRS J. Photogramm. Remote Sens. 146, 436–452. https://doi.org/10.1016/j.isprsjprs.2018.10.010.

Yang, D.i., et al., 2017. Open land-use map: a regional land-use mapping strategy for incorporating OpenStreetMap with earth observations. Geo-spatial Inf. Sci. 20, 269–281. https://doi.org/10.1080/10095020.2017.1371385.

Freire, S., et al., 2019. GHSL Data Package 2019 Public release. European Commission, Joint Research Centre https://www.doi.org/10.2760/0726.

Goodchild, M.F., 2007. Citizens as sensors: the world of volunteered geography. GeoJournal 69, 211–221. https://doi.org/10.1007/s10708-007-9111-y.

Gorelick, N., et al., 2017. Google Earth Engine: planetary-scale geospatial analysis for everyone. Remote Sens. Environ. 202, 18–27. https://doi.org/10.1016/j.rse.2017.06.031.

Herold, M., Roberts, D. A., 2010. The spectral dimension in urban remote sensing. In: Rashed, T., Jürgens, C. (Eds.). Remote sensing of urban and suburban areas, Remote Sens. and Digital Image Processing. 10, 47-65. Doi: 10.1007/978-1-4020-4385-7_4.

Jensen R, John, 2016. Introductory Digital Image Processing: a remote sensing perspective, 4th. Pearson Education.

Liu, D., et al., 2020. Annual large-scale urban land mapping based on Landsat time series in Google Earth Engine and OpenStreetMap data: A case study in the middle Yangtze River basin. ISPRS J. Photogrammetry Remote Sens. 159, 337–351. https://doi.org/10.1016/j.isprsjprs.2019.11.021.

Lu, D., Weng, Q., 2007. A survey of image classification methods and techniques for improving classification performance. Int. J. of Remote Sens. 28, 823–870. https://doi.org/10.1080/01431160600746456.

Mesev, V., 2010. Classification of urban areas: inferring land use from the interpretation of land cover. In. Rashed, T., Jürgens, T. (Eds.). Remote Sensing of Urban and Suburban Areas. Remote Sens. and Digital Image Processing. 10. Doi: 10.1007/978-1-4020-4385-7_8.

Pesaresi, M., et al., 2016. Assessment of the added-value of sentinel-2 for detecting built-up areas. Remote Sens. 8 https://doi.org/10.3390/rs8040299.

Qiao, L., et al., 2019. The identification and use efficiency evaluation of urban industrial land based on multi-source data. Sustainability. 11, 6149. https://doi.org/10.3390/su11216149.

Ridd, M.K., 1995. Exploring a V-I-S (vegetation-impervious surface-soil) model for urban ecosystem analysis through remote sensing: comparative anatomy for cities. Int. J. of Remote Sens. 16, 2165–2185. https://doi.org/10.1080/01431169508954549.

Rizzini, C.T., 1997. Tratado de Fitogeografia do Brasil: aspectos ecológicos, sociológicos e florísticos, 2nd ed. Âmbito Cultural, Rio de Janeiro.

Rouse, J.W., et al., 1973. Monitoring vegetation systems in the great plains with ERTS. Third Earth Resources Technology Satellite (ERTS) Symposium 1, 309–317.
Silva, D.V.S., Cruz, C.B.M., 2018. Caatinga typologies: a review to support mapping through orbital remote sensing and GEOBIA. Revista do Departamento de Geografia. 35, 113–120. https://doi.org/10.11606/rdg.v35i0.142710.
Souza, C., et al., 2020. Reconstructing three decades of land use and land cover changes in brazilian biomes with landsat archive and earth engine. Remote Sens. 12 https://doi.org/10.3390/RS12172735.
Stone, K.H., 1965. The Development of a Focus for the Geography of Settlement. Econ. Geography. 41, 346–355. https://doi.org/10.2307/141945.
Sun, J., et al., 2020. Mapping essential urban land use categories in nanjing by integrating multi-source big data. Remote Sens. 12, 2386. https://doi.org/10.3390/rs12152386.
Venturi, L.A.B.V., 2021. Recursos Naturais do Brasil. Appris, Curitiba.
Wentz, E.A., 2014. Supporting global environmental change research: a review of trends and knowledge gaps in urban remote sensing. Remote Sens. 6, 3879–3905. https://doi.org/10.3390/rs6053879.
Xu, H., 2006. Modification of normalised difference water index (NDWI) to enhance open water features in remotely sensed imagery. Int. J. Remote Sens. 27, 3025–3033. https://doi.org/10.1080/01431160600589179.
Zhang, H., et al., 2020. Extracting Impervious Surface from Aerial Imagery Using Semi-Automatic Sampling and Spectral Stability. Remote Sens. 12, 506. https://doi.org/10.3390/rs12030506.
Zhao, W., et al., 2019. Exploring semantic elements for urban scene recognition: Deep integration of high-resolution imagery and OpenStreetMap (OSM). ISPRS J. Photogramm. Remote Sens. 151, 237–250. https://doi.org/10.1016/j.isprsjprs.2019.03.019.
Zhao, Y., et al., 2022. ASI: An artificial surface Index for Landsat 8 imagery. Int. J. Appl. Earth Observation Geoinformation. https://doi.org/10.1016/j.jag.2022.102703.
Zhong, Y., et al., 2020. Open-source data-driven urban land-use mapping integrating point-linepolygon semantic objects: a case study of Chinese cities. Remote Sens. Environ. 247 https://doi.org/10.1016/j.rse.2020.111838.
Zhu, Z., et al., 2019. Understanding an urbanizing planet: Strategic directions for remote sensing. Remote Sens. Environ. 228 https://doi.org/10.1016/j.rse.2019.04.020.